The isolated Wuchiapingian (Zechstein) Wielichowo Reef and its sedimentary and diagenetic evolution, SW Poland

Adam FHEED[1, *], Anna ŚWIERCZEWSKA[1] and Artur KRZYŻAK[1]

[1] AGH University of Science and Technology, Faculty of Geology, Geophysics and Environmental Protection, Department of Fossil Fuels, al. A. Mickiewicza 30, 30-059 Kraków, Poland

The development of a relatively small and isolated part of the Wuchiapingian, Zechstein Wielichowo Reef was possible owing to a progressive subsidence and frequent sea level fluctuations. Three biofacies were distinguished within this feature: (1) the shallow-water and highly energetic *Acanthocladia* biofacies, dominated by bryozoans and crinoids, with poorly preserved porosity, reduced mainly by calcite cementation and compaction; (2) the *Horridonia* biofacies comprising numerous brachiopods preferring a moderate depth of water, with comparably poor porosity; and (3) the *Fenestella/Kingopora* biofacies rich in the most highly variable fossils, of the deepest and calmest waters, occurring at the top of the section and showing a significant effective porosity, reaching almost 13%. Among many diagenetic processes altering the reef, several lines of evidence suggest that it was the meteoric diagenesis to enhance its porosity most extensively. Since no stromatolites are present, the final sea level drop is interpreted to be rapid, hence creating conditions favourable for the meteoric dissolution. Some intraparticle porosity, however, seems to be of depositional origin.

Key words: reef, microfacies, diagenesis, porosity, Zechstein Limestone, Wolsztyn Ridge.

INTRODUCTION

During Permian times, western Poland was part of the Southern Permian Basin (Fig. 1A) that developed due to rifting on a considerable scale (Gast, 1988; Pharaoh et al., 2010). Its basement is built of folded Devonian and Carboniferous rocks (Kiersnowski et al., 2010). The main development of this basin took place between the Carboniferous and Permian when a complex network of horsts and grabens was formed due to extensional movements (Ziegler, 1990; Kiersnowski et al., 2010). In the eastern part of the Southern Permian Basin, there is an uplifted pre-Zechstein horst structure, the Brandenburg–Wolsztyn–Pogorzela Palaeo-High (or shortly, Wolsztyn Ridge or Wolsztyn–Pogorzela High; Dyjaczyński et al., 1997; Dyjaczynski et al., 2001; Kiersnowski et al., 2010; Fig. 1B). It is the place where numerous reef bodies (Fig. 1B, C) with beneficial petrophysical parameters have been developed (Dyjaczyński et al., 1997; Dyjaczynski et al., 2001; Kotarba et al., 2006; Kiersnowski et al., 2010; Peryt et al., 2012a). Consequently, they host gas deposits. The adjacent basinal zones abound in thin carbonate facies (e.g., Peryt and Ważny, 1980; Peryt, 1981; Dyjaczyński et al., 1997, Reijers, 2012; Dyjaczyński and Peryt, 2014; Peryt et al., 2015) that rarely ex-

ceed 5 m in thickness (Dyjaczyński et al., 1997; Pikulski and Wolnowski, 2005). The main factor that controlled the growth of the reefs was associated with the subsidence, which tended to be progressive and controlled by a consequent sea level rise (Strohmenger et al., 1996).

The biota found within the reefs of western Poland are typical bryonoderm (cold-water) organisms (Peryt et al., 2012a), as the Zechstein basin, during Wuchiapingian times, was inundated by cold waters of the Barents Sea (D. Peryt et al., 2012; Peryt et al., 2012a, b). The aim of this paper is to characterise the development of a relatively small, isolated reef body recorded in the Wielichowo-8 borehole, located north of the larger and better documented, Wielichowo Reef (Fig. 1C). The Wielichowo Reef is about 5 to 6 km long and 0.5–1 km wide (Dyjaczyński et al., 1997). The feature studied, formally being a part of the Wielichowo Reef (Tomaszewska et al., 2008, unpubl.), occurs close to the Ruchocice Reef (Fig. 1C). It represents the PZ1 (Werra) cyclothem within which the Zechstein Limestone (Ca1) carbonates developed, followed by sulphate deposits. The outlines of all these reefs were interpreted on the basis of 3D seismic research (e.g., Dyjaczynski et al., 2001; Kiersnowski et al., 2010).

The combination of microscopic and Nuclear Magnetic Resonance (NMR) studies allowed us to characterise the petrophysics of the Zechstein Limestone reservoir, and hence created a possibility to determine an influence of both diagenesis and deposition on pore space evolution. The history of the isolated reef helps to understand the reservoir variability in larger reef complexes, occurring in the Southern Permian Basin.

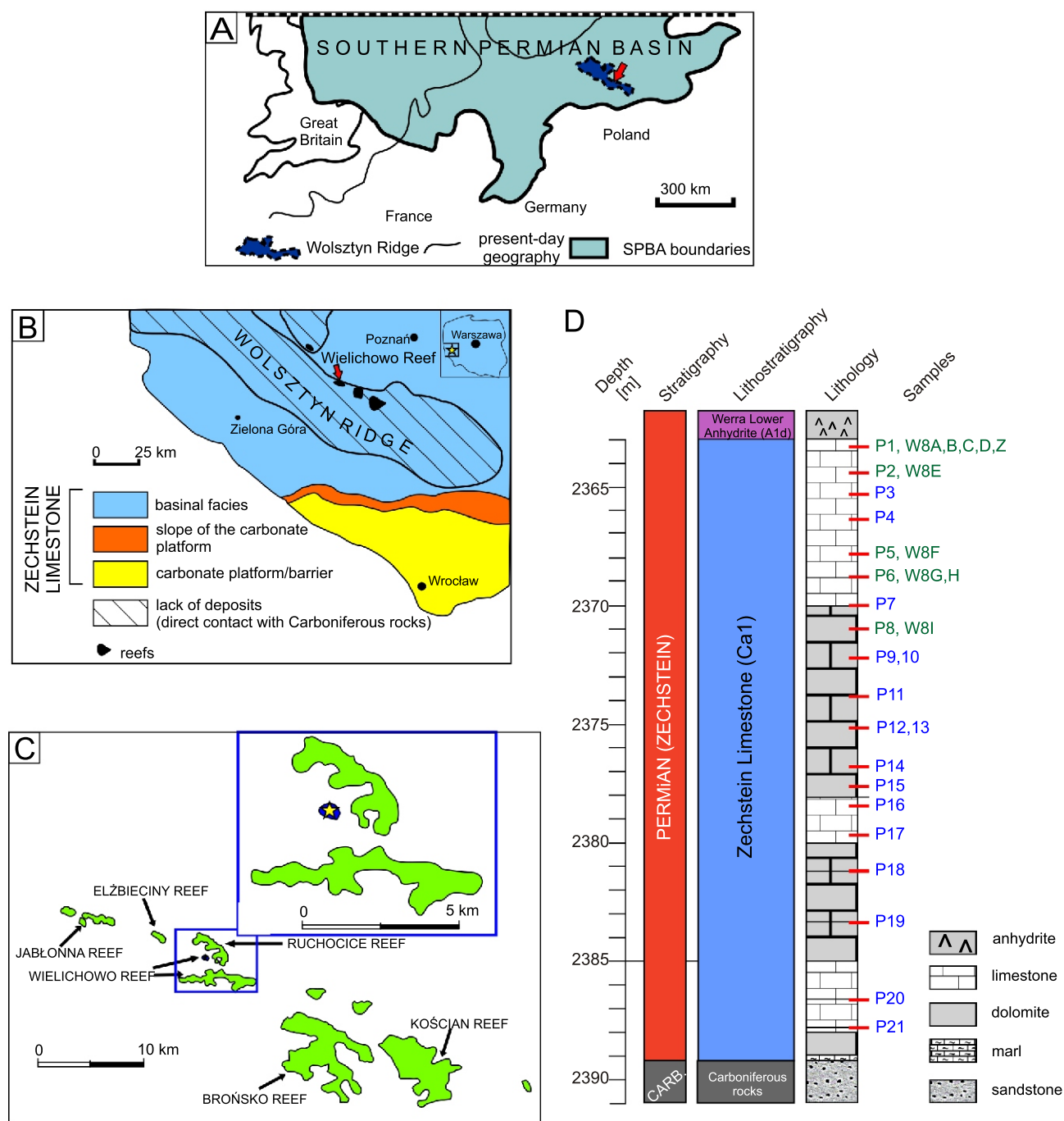* Corresponding author, email: adam.fheed@gmail.com

Fig. 1. Location of the studied reef

A – present-day geography and former Southern Permian Basin (SPBA) boundaries after Smith (1980, modified; red arrow indicates location of the reef); **B** – reefs of the Wolsztyn Ridge (western Poland; location marked by yellow asterisk) after Karnkowski (1999, modified); **C** – interpretation of the Wolsztyn reefs boundaries after Wilk (2008, Geofizyka Toruń, unpubl., modified) and Tomaszewska et al. (2008, PGNiG SA, unpubl.); **D** – simplified lithostratigraphy of the studied reef (Wielichowo-8 borehole); P – main sample, W – supplemental sample

MATERIAL AND METHODS

Preliminary carbonate facies were distinguished based on macroscopic core description. Besides macroscopic observations, 32 samples of rocks for thin section preparation were collected to enhance the previous research (Fig. 1D). They were studied under a polarizing microscope in transmitted light to identify their mineral composition, textural arrangement and to recognize the presence of fossils and cements within the samples. The textures of the rocks were described based on the

scheme of carbonate divisions proposed by Dyjaczynski et al. (2001) for reef rocks from this part of the basin, whereas the biofacies were characterized on the basis of earlier microfacies classification for the reefs from the Wolsztyn Ridge (Raczyński, 2000; Peryt et al., 2012a). Core description, and microscopic observations were undertaken using Dunham (1962) classification of carbonate rocks. In addition, cathodoluminesce studies were carried out. The voltage of the equipment was equal to 15 kV, while the current intensity was set to 350 mA.

The characterization of the subsequent generations of cements was supported by using the backscattered SEM microscopy. The SEM studies were accompanied by the EDS module, allowing the mineral composition recognition. Two bulk rock samples and nine samples of sulphates were analysed by X-ray diffraction (XRD), in order to distinguish anhydrite from gypsum. Moreover, the Alizarin Red S and Potassium Ferricyanide composite test was made to ensure the identification of dolomite and calcite, respectively, as well as potential iron content. The solution was prepared according to Evamy (1963) recipe.

For the purposes of NMR (Nuclear Magnetic Resonance) studies, the cylindrical cores of 1 and 1.5 inch in width and length, respectively, were collected. The NMR was undertaken to provide a quantitative porosity study. An external magnetic field strength was equal to 50 mT, the wait time (TW) was set to approximately 1 s, and the inter-echo spacing (TE) corresponded to an interval between 30–50 s. The investigation was based on T2 relaxation time, associated with the loss of magnetisation in a transverse plane (perpendicular to the static magnetic field) – e.g., Akkurt et al. (2009). The magnetisation is related to the hydrogen nuclei, whose spins orient themselves along a particular direction pointed by the magnetic field (Coates et al., 1999). According to the cited author, there is a correlation between the size of the pores and the T2 relaxation time. The smaller a particular void is, the shorter T2 time it exhibits. The T2 value is used to separate movable fluids from irreducible ones (Akkurt et al., 2009; Coates et al., 1999). The porosity expressed by the occurrence of movable fluids corresponds to the FFI – Free Fluid Index, while the MCBW – Clay-Bound Water and BVI – Bulk Volume Irreducible (here: capillary water) correspond to the spaces excluded from free motion of fluids (Coates et al., 1999). The effective NMR porosity (MPHI) is counted as a sum of BVI and FFI, while the MSIG stays for the total NMR porosity (Coates et al., 1999). Moreover, to ensure that the genetic aspect of the encountered porosity is considered, it was characterized on the basis of Choquette and Pray (1970) classification. The shape and the form of the pores have been used to distinguish between the primary and secondary porosity.

RESULTS AND INTERPRETATION

LITHOLOGY

The section (from bottom to top) starts with marls (Figs. 1D and 2). The reef is documented at a depth ranging from 2363 to 2389 m. A very strong dolomitisation of the reef occurs at the following depth intervals: 2388–2389, 2380–2385 and 2370–2378 m (Fig. 1D). The Zechstein Limestone (Ca1) is bounded by the Lower Anhydrite (A1d) sulphates and Carboniferous sandstones from the top and from the bottom, respectively (Fig. 1D).

FACIES ANALYSIS

The studied reef shows quite a wide diversity of both textural arrangement of rocks and fossil evidence (Figs. 2–4). On the basis of the textural differentiation, six units (designated A–F) have been distinguished (Fig. 2), whereas the variability of fossils allowed us to assign three biofacies: (1) the *Acanthocladia* biofacies, dominated by bryozoans, occurring most frequently; (2) locally observed *Horridonia* biofacies, containing numerous brachiopods; and (3) the uppermost, strongly diversified *Fenestella/Kingopora* biofacies, represented by a wide range of fossils.

The lowest part of the section, i.e. unit A, is slightly marly and contains only sparsely distributed fossils – mainly bryozoans, characteristic for the major part of the reef. Its thickness is relatively small and does not exceed 20 cm (Figs. 1D and 2). Such marly sediments often occur also in the southern part of the Polish Southern Permian Basin (e.g., Biernacka et al., 2005). As bryozoans showing strongly fragmented zoaria are abundant within this interval, it may be classified as the *Acanthocladia* biofacies (cf. Figs. 3A, D and 4B). This is because the bryozoans of this biofacies are very delicate and sporadically preserved without any damage (e.g., Raczyński, 2000; Peryt et al., 2012a; Fig. 3A).

Unit A is overlain by a 3 m thick complex of bindstones (unit B; Fig. 3A, B). Although the term "bindstone" was found appropriate in terms of the textures, they show a similarity with grainstones, some of which are dolomitised (Fig. 1D). They are grain-supported and lacking of carbonate mud. Unit B also represents the *Acanthocladia* biofacies and the bryozoans of this unit show a characteristic pinnate form, more extensively discussed by Hara et al. (2013) and Raczyński (2000; cf. Fig. 3A). The *Acanthocladia* biofacies continues upwards from the bottom of the Zechstein Limestone (2389.2 m) to a depth of 2385 m. In the interval 2386–2388 m, the bryozoans are accompanied by *Horridonia* (Figs. 3B and 4A). Additionally, crinoids are also very frequent (Figs. 3C, D and 4B).

Unit B is covered by an ~8 m thick complex dominated by dolograinstones (Figs. 2 and 3C) of unit C, with intercalations of bindstones and packstones/rudstones. These rocks can be referred to as bioclastic grainstones and packstones with anhydrite. From the palaeontological point of view, this division begins with the *Acanthocladia* biofacies, characterized by a considerable addition of crinoids (Figs. 3C and 4B). Towards the top, bryozoans become the second skeletal component after the crinoids. Then, at a depth of approximately 2385 m, it turns into the *Horridonia* biofacies (Figs. 3B and 4A), and finally, again changes back into the *Acanthocladia* biofacies. The final transition from the *Acanthocladia* to *Horridonia* biofacies takes place at a depth of 2382 m. Within unit C sulphate rocks are common, too.

Unit D starts with dolowackestones (Fig. 3D) and local packstones. The top of this unit has hardly recognizable depositional textures (no visible fossils), and thus was classified as a crystalline rock – dolomite in this case (Figs. 1D and 3E). Nevertheless, it contains sparsely distributed stems of crinoids (Fig. 4B). Within the packstone intercalations, the crinoids are frequently accompanied by bryozoans and foraminifers. However, the number of bryozoans does not exceed the amount of crinoids. The co-occurrence of strongly fragmented *Acanthocladia* and crinoids suggests the presence of the *Acanthocladia* biofacies with numerous crinoids.

Unit E is 5 m thick and changes upwards from dolomite to limestone (Fig. 1D). It begins with dolowackestones/packstones passing into slightly better packed rocks, represented by typical dolopackstones (Fig. 3F). It is richer in fossils than the previous ones (Figs. 2, 3F and 4B). The fossils at the bottom of this unit comprise crinoids and gastropods, replaced upwards by bryozoans, brachiopods, bivalves (Fig. 3F) and locally preserved foraminifers (Fig. 2). Variable fossils indicate a close neighbourhood of the *Fenestella/Kingopora* biofacies (Figs. 3F, H and 4C–E). At a depth of approximately 2374 m, intraclastic breccia was identified (Fig. 3G). The breccia contains clay minerals and detrital quartz and is strongly affected by physical compaction. Near the top of unit E, *Strophomenata* brachiopods, with characteristic thick shells, start to appear
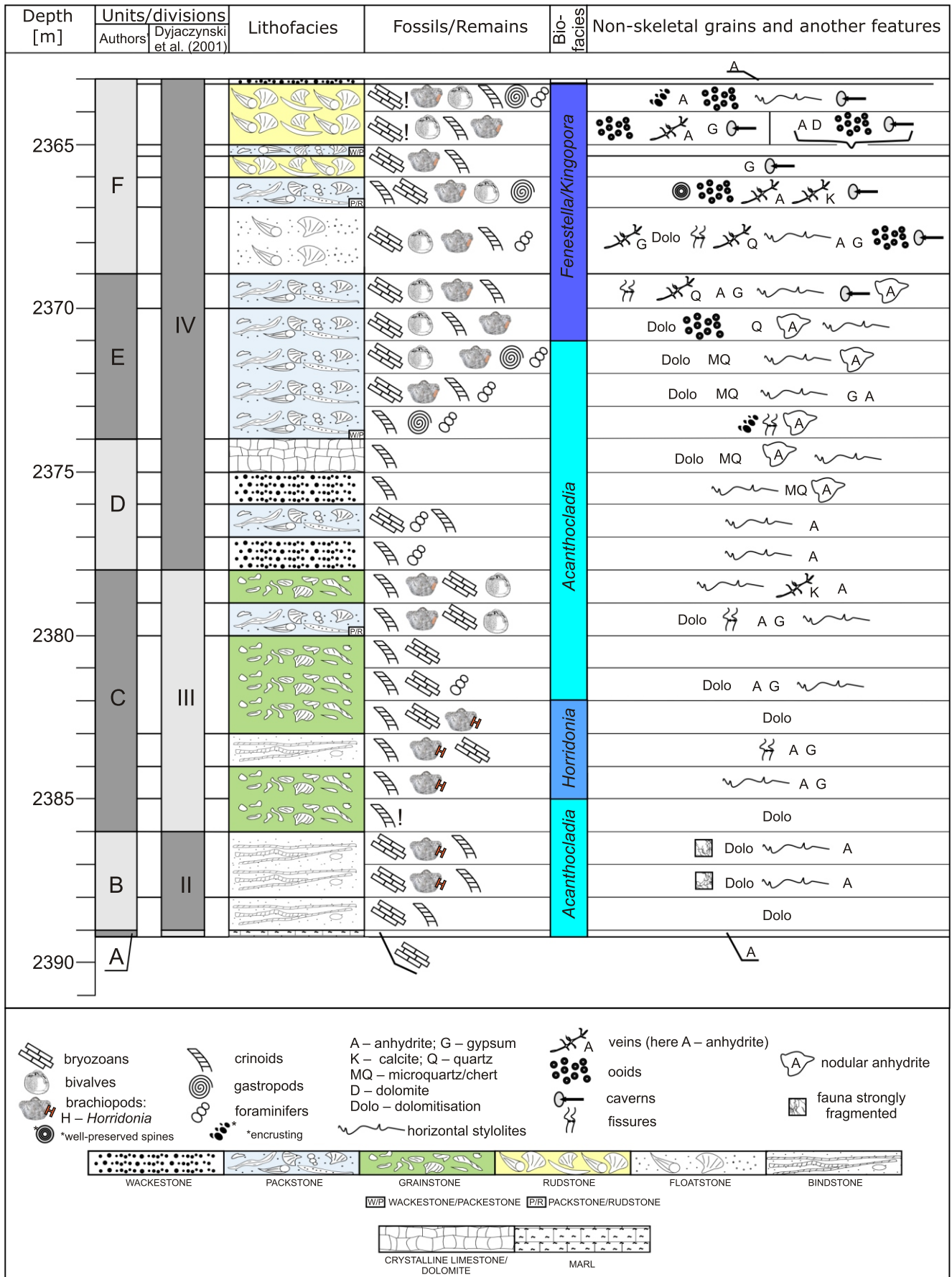
Fig. 2. A litho- and biofacies/microfacies section of the Zechstein Limestone (Ca1) within the reef (Wielichowo-8 borehole)

A–F – textural subdivisions: **A** – marly carbonates, **B** – bindstones, **C** – grainstones with intercalations of bindstones and packstones/rudstones, **D** – wackestones, packstones and crystalline dolomites, **E** – packstones and wackestones/packstones, **F** – mainly rudstones; **II–IV** – biofacies divisions distinguished based on Dyjaczynski et al. (2001): **II** – bioclastic grainstones with extraclasts; **III** – bioclastic grainstones and packstones (frequently with anhydrite); **IV** – bioclastic wackestones/grainstones with intraclastic breccia and carbonate laminae
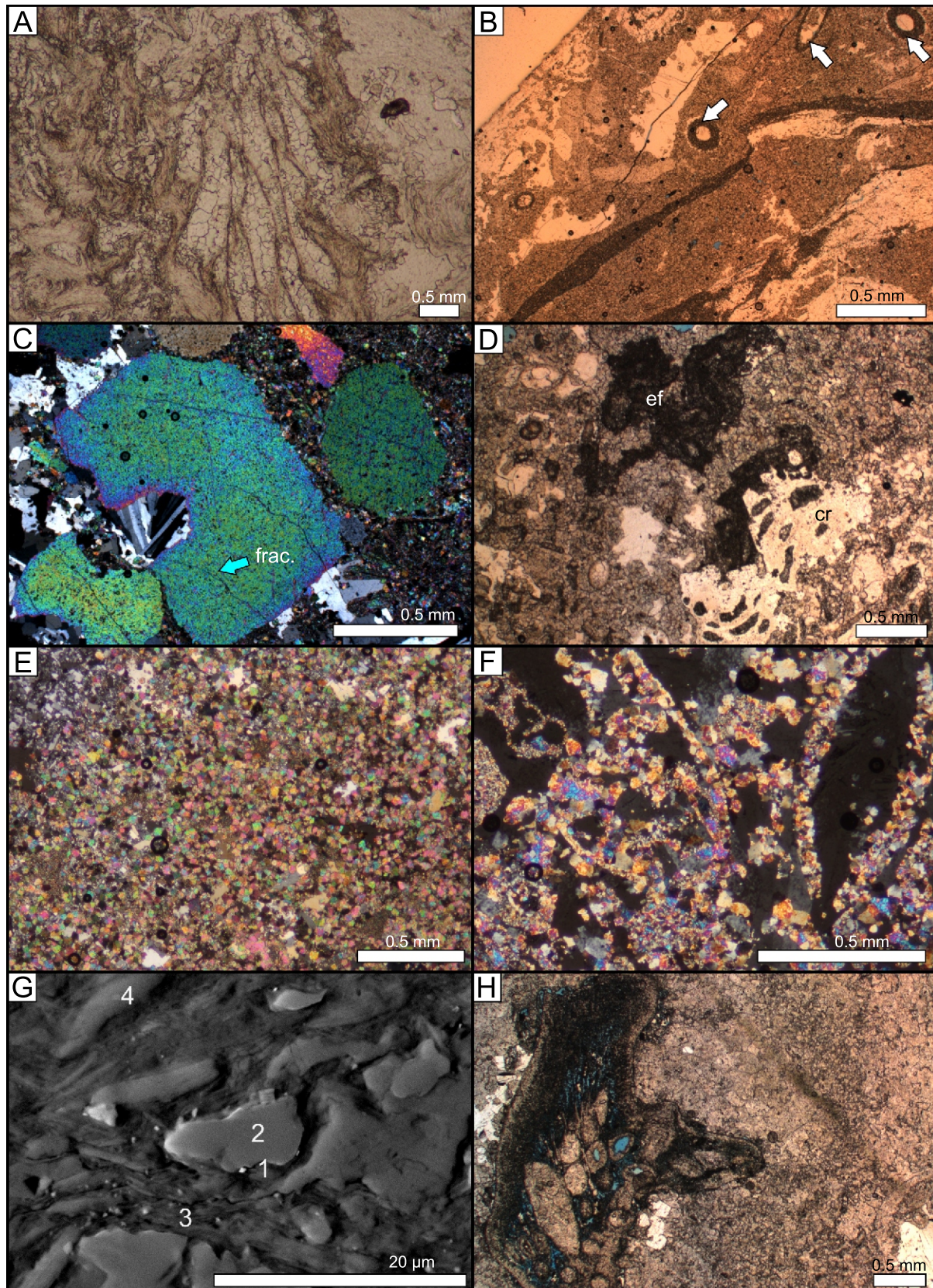
Fig. 3. Biofacies and textural arrangement of the rocks studied, fossils of the three biofacies

A – bryozoan of the *Acanthocladia* biofacies bindstone of unit B; **B** – *Horridonia* brachiopod and its spines (arrowed) in unit C, anhydrite-rich bindstone (anhydrite is white); **C** – crinoids of the *Acanthocladia* biofacies cut by open fractures (arrowed) – grainstone of unit C; **D** – *Acanthocladia* encrusted by foraminifers and fragments of crinoids replaced by anhydrite – wackestone of unit D; **E** – dolograinstone with anhydrite of unit D; **F** – bivalves of the *Fenestella/Kingopora* biofacies packstone of unit E, showing intraparticle porosity (black); **G** – matrix of intraclastic breccias of unit E; **H** – bryozoans of the *Fenestella/Kingopora* biofacies – rudstone of unit F – note intraparticle porosity (blue); A, B, D, H – plane-polarized light; C, E, F – cross-polarized light; G – backscattered electron microscope photograph; cr – crinoids, ef – encrusted foraminifers, frac. – open fracture; 1 – heavy minerals, 2 – detrital quartz, 3 – clay minerals, 4 – dolomite
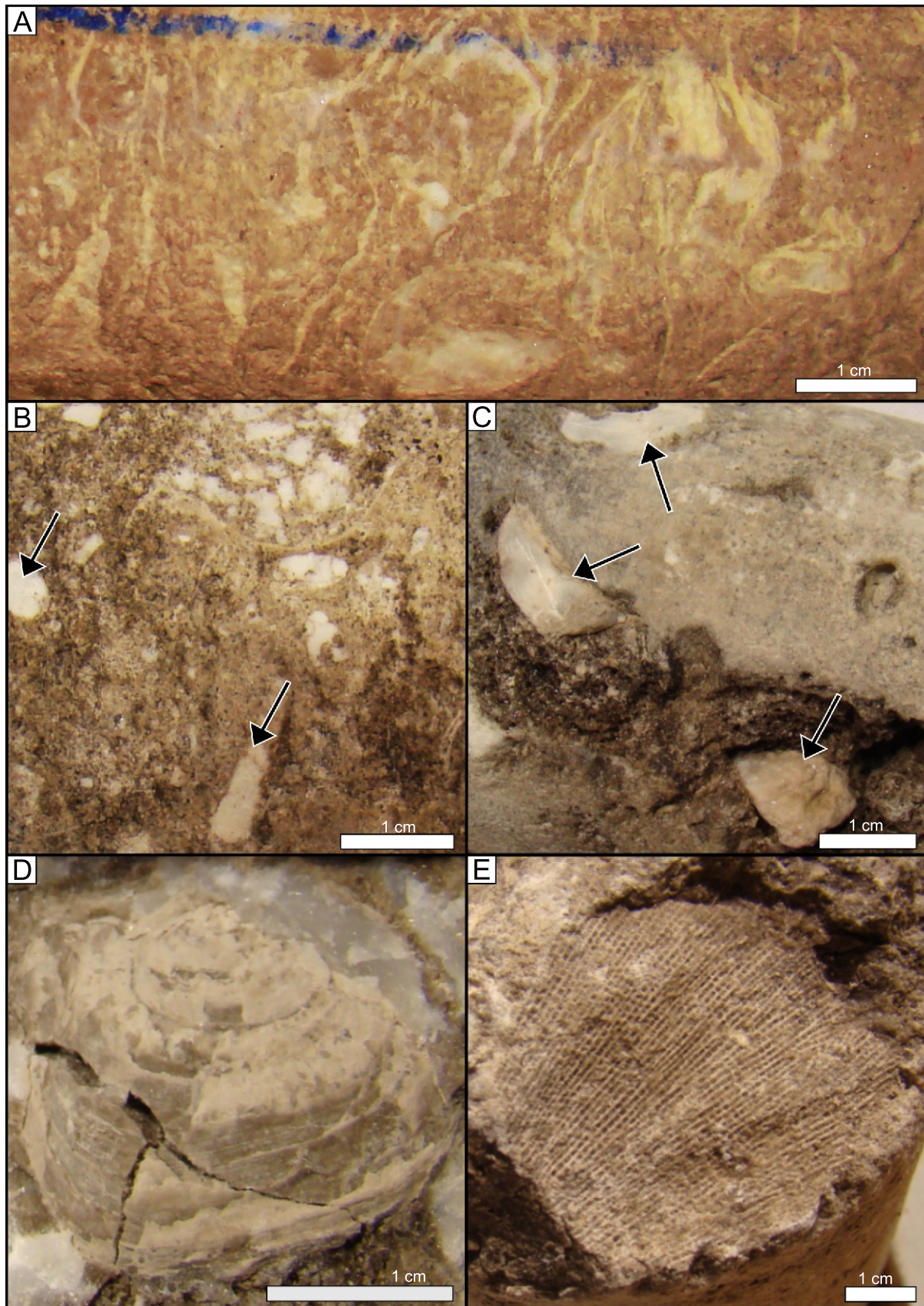
Fig. 4. Fossils of various biofacies

A – *Horridonia* biofacies (brachiopods); **B** – crinoids of *the Acanthocladia* biofacies (arrowed); **C–E** – *Fenestella/Kingopora* biofacies: **C, D** – thick shells of *Strophomenata* brachiopods (arrowed) – note large dissolution caverns on C; **E** – reticulate bryozoan

(Fig. 4C, D). Their highest frequency corresponds to the interval between 2368 and 2372 m. They remain present up to the top boundary of the Zechstein Limestone, and are surrounded by numerous bryozoans that become increasingly larger in size towards the top (Fig. 4E). Because the majority of unit E is still showing numerous fragmented bryozoans, it can be treated rather as the *Acanthocladia* biofacies with signs of transition into the *Fenestella/Kingopora.*

Unit F contains rocks ranging in types from floatstones, through packstones/rudstones and wackestones/packstones, to typical rudstones (Figs. 2, 3H and 4C–E). Their characteristic feature is also carbonate mud co-occurring with the sparry cement. The top of this unit terminates with a 12 cm of a wackestone, and its overall thickness is 6 m (Fig. 2). In contrast to unit E, the *Fenestella/Kingopora biofacies* is undoubtedly present within unit F (Figs. 2, 3H and 4C–E). The preservation of fossils is considerable within the whole unit. It means that they are only slightly fragmented and their shells are relatively thick (Fig. 4C–E) – thus justifying the division of rudstones. The fossils do not show any signs of reworking. The top boundary of unit F is sharp, rather than gradual, however, a thin layer characterized by the appearance of both limestone and anhydrite (a part of the Werra Lower Anhydrite A1d) occurs at a depth of 2363.5 m (Fig. 1D).

An attempt was undertaken to correlate the obtained results with the already existing classification of carbonate rocks of the Kościan–Wielichowo region. The marly unit A, has no equivalent in the Dyjaczynski et al. (2001) subdivision (cf. Fig. 2). Unit B corresponds to the (II) unit of Dyjaczynski et al. (2001), i.e. to bioclastic grainstones with extraclasts. Unit C can be treated as bioclastic grainstones and packstones (III unit). Finally, the bottom of unit D, forms a boundary between the general units (III) and (IV). This means that wackestones-grainstones with intraclastic breccia and abundant rudstones (unit IV) generally appear above the depth of 2378 m in the studied section. Both the lowermost and uppermost units (I and V) are missing and these are the carbonate breccia and the stromatolitic-pisolitic unit, respectively.

CEMENTATION AND OTHER DIAGENETIC ALTERATIONS

Among many different zones of the section, cementation variability can be noticed. Calcite, dolomite and anhydrite can be seen the most frequently. The majority of cements and minerals display both yellow and brown luminescence. This applies mostly to the zonal, sparry crystals of calcite. Moreover, red or slightly brownish luminescence corresponds mainly to dolomite. The sulphates, in turn, show either dark brown or no luminescence. Fluorite, in the form of both replacive crystals and cements is blue in cathodoluminescence, and occurs along the entire section. Its abundance increases systematically towards the top.

Multiphase recrystallisation was common within the reef. It is exhibited by the fact that the mosaic of calcite and/or dolomite is strongly diversified in terms of crystal sizes. It happens that some crystals are close to a medium-crystalline calcite/dolomite, whereas others reach a size of typical sparite.

Unit B. The cements of bioclastic grainstones can be divided into at least five generations (Fig. 5A, B). The oldest generation is calcite of brown luminescence, forming needle-like fringes, locally observed also within the botryoidal fans (1) (Fig. 5A–D). It surrounds two subsequent generations of equant calcite, showing yellow to brown luminescence (2, 3). The innermost parts of the strongly fragmented fossils are filled by a red generation of dolosparite (4).

Locally, even two generations of dolomite were recognized. They are marked by the luminescence varying from red to brown (Fig. 5A). The dolomite mosaic can be treated as medium-crystalline dolosparite (Fig. 5C). Finally, the fluorite cement precipitated (5; see Fig. 5B). Another important feature of unit B is horizontal stylolites. Here, they are most abundant among all the studied units (Fig. 5C). The petrographic situation within unit B is additionally supplemented by the occurrence of anhydrite, that either forms the cement or partially crystallises inside the stylolites (Fig. 6A).

Unit C. A little bit upper, where the rocks of grainstone-dominated unit C appear (Figs. 2 and 3B, C), six generations of cements were distinguished (Figs. 5E, F and 7A–D). Anhydrite, showing weak luminescence, was the first that precipitated (1). At few places, it co-occurs with gypsum, that appears too rarely to be considered as a separate cement generation. Then, red, fine-crystalline dolosparite precipitated (2; Fig. 5E, F). Subsequently, the zonal calcite composed of yellow and brown bands with sharp curvature replaced the interiors of crinoids (3; Figs. 5E, F and 7A–D). The next generation of cement represented by equant calcite of brown to yellow luminescence occurred on their contours (4; Fig. 7A, B). Then, dolosparitic crystals precipitated (5; Fig. 5E, F). The dolosparite is increasingly frequent towards the top of the section. Finally, the fluorite cements of blue luminescence developed (6) and significantly decreased the intercrystalline porosity (Fig. 7B). It is worth adding, that all of these generations are cut by numerous open fractures (rarely filled with anhydrite), whose appearance is interpreted to be the latest (Fig. 5E, F). The stylolites, although not observed under the polarizing microscope, were clearly visible on a macroscopic scale (cf. Fig. 2).

Unit D. The weakly luminescent, foraminifera-rich wackestones of unit D, comprise four basic generations of cements (Fig. 7E–H). They occur in the following, chronological order: red, fibrous dolomite (1); brown, fibrous calcite (2); anhydrite lacking luminescence (very dark red), occurring among the dolosparite mosaic (Fig. 7B) in the form of both veins and patches, as well as cement filling the chambers of foraminifers (3); and the blue fluorite cement (4). The fluorite crystals fill the intercrystalline pores (Fig. 7F, H). These wackestones, similarly as in case of unit C, are often cut by fractures. Because they are commonly filled by anhydrite, they usually do not account for the total porosity observed within this interval. Moreover, numerous horizontal stylolites were observed (Figs. 2 and 6B).

Unit E. Within unit E, the amount of calcite increases, especially at a depth of 2371 m (Fig. 8). It is expressed by brown luminescence. Here, the sparry, needle calcite (1) was postdated by a selectively precipitating generation of red dolosparite (2). This, in turn, was followed by another generation of sparry calcite (3; see Fig. 8A–D). In the remaining part of unit E (above and below 2371 m depth), another set of cements was noted (Fig. 8E–H). Firstly, red, fine-crystalline dolosparite appeared within the remnants of the biota (I). Then, it was postdated by the appearance of poorly luminescent, acicular gypsum (II) (Fig. 8E, F). Although gypsum appears relatively frequently within unit E, it is much less common than anhydrite, as confirmed by XRD analyses. Gypsum (Fig. 6C) is often found in the shells of bivalves and gastropods, as presented in Figure 8E. Greater amount of anhydrite, in turn, was observed in the form of nodules – clearly visible in the core section (Fig. 6A), as well as within formerly developed intercrystalline porosity. The appearance of sulphates, was followed by the precipitation of dolosparite (III; Fig. 8E–H). Subsequently, two varieties of calcite cements were formed: zonal calcite cements (IV) of luminescence ranging from yellow to brown (Fig. 8G, H); and
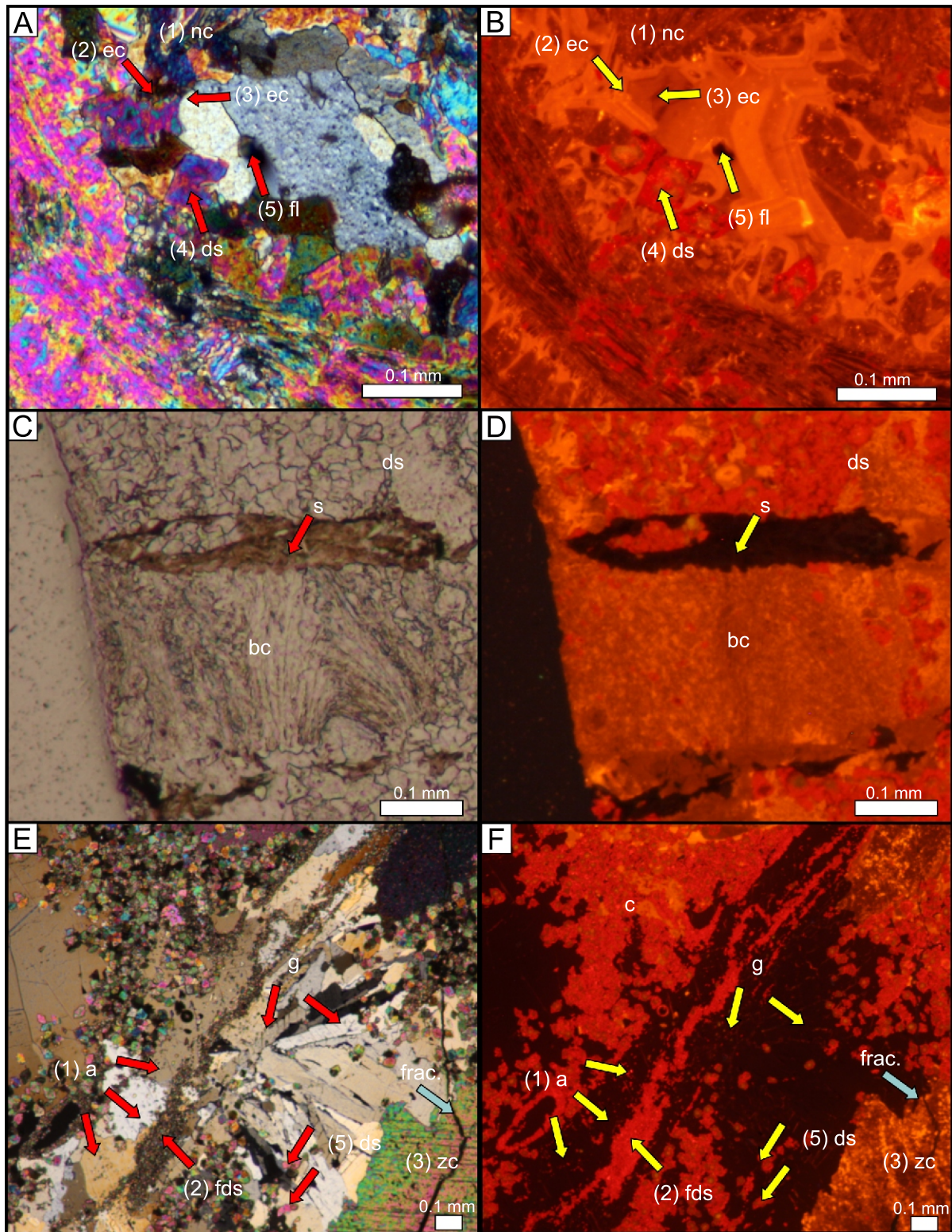
Fig. 5. Cementation and other diagenetic alterations in units B and C

A, B – five subsequent cement generations of unit B, B – note two generations of dolomite (brownish inside a red mass); C, D – post-aragonitic botryoidal fans of unit B (now calcite), accompanied by a stylolite; E, F – fractured rock and cement generations of unit C – note early sulphate precipitation and polyphase dolomite crystallisation; A, E: cross-polarized light; C – plane-polarized light; B, D, F – cathodoluminescence; (1) corresponds to the oldest cement generation; a – anhydrite, bc – botryoidal calcite, ds – dolosparite, ec – equant calcite, fds – fine-crystalline dolosparite, fl – fluorite, g – gypsum – note a specific orientation of cleavage in photograph E (left arrow), nc – needle-like calcite, S – stylolite, zc – zonal calcite; other explanations as in Figure 3
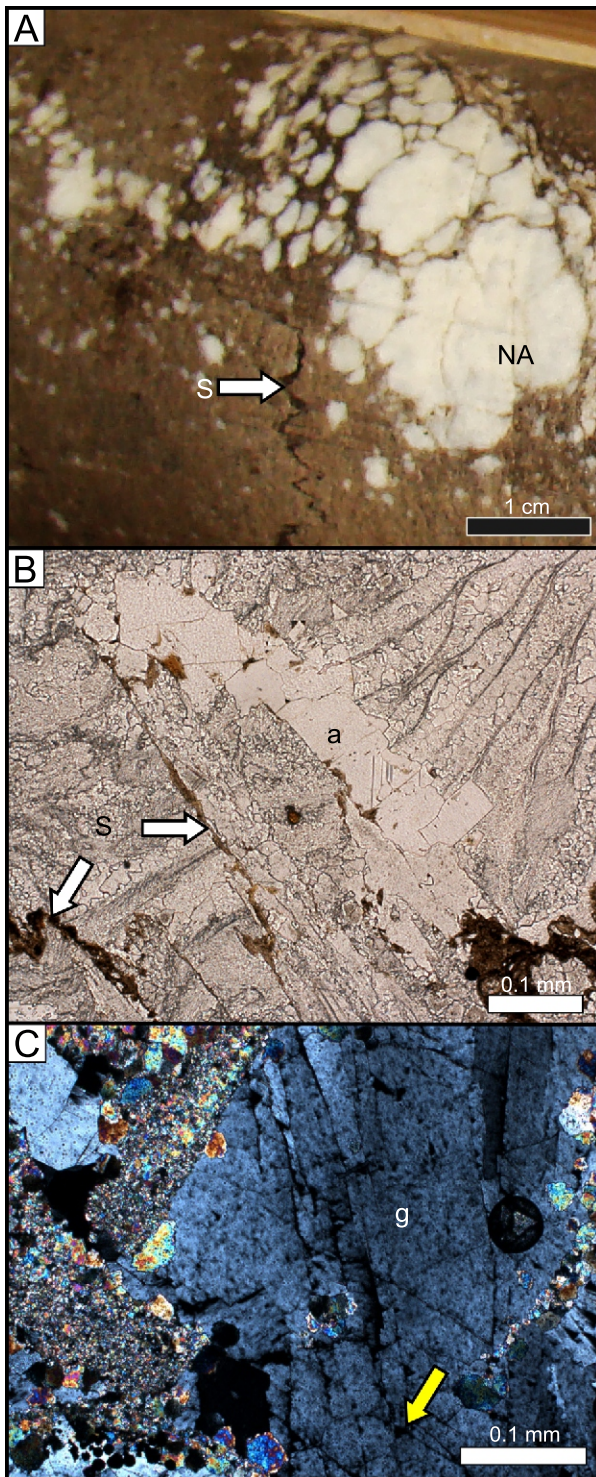
Fig. 6. Sulphates

A – nodular anhydrite deposited in a sabkha environment, post-dated by chemical compaction marked by a stylolite (arrowed); **B** – anhydrite cement postdating the chemical compaction structures (arrowed); **C** – an example of a gypsum crystal with clearly visible cleavage (yellow arrow); A – core photograph; B – plane-polarized light; C – cross-polarized light; NA – nodular anhydrite, S – stylolite; other explanations as in Figure 5

poikilitic calcite of light yellow luminescence (V; Fig. 8E, F). After the formation of these cements, sparry fluorite crystals appeared (Fig. 8C, D). Micrite, and especially dolomicrite, is found frequently here, which is, in general, a characteristic feature of packstones (Dunham, 1962). Another property of unit E, is the occurrence of the previously mentioned intraclastic breccia (Fig. 3G). The breccia occurs at the bottom of the unit and comprises minerals showing diverse luminescence – from red, through brown and yellow, even to green. The SEM EDS module has yielded information about its chemical composition. In this particular case, yellow and brown colours indicate clay minerals and locally occurring detrital quartz grains, while green luminescence is related to heavy minerals. Besides, rarely distributed crystals of dolomite were also identified. The evidence of both chemical (dissolved quartz grains) and physical compaction (fractured contours, squeezed minerals: see Fig. 3G) are noticeable inside the breccia. Both fractures and horizontal stylolites are of a negligible significance within unit E.

Unit F. The uppermost textural subdivision – unit F, represented mainly by rudstones (Figs. 2, 3H and 4C–E), shows a dominance of calcite cements, with brown luminescence. The occurrence of red-luminescent dolomite is usually limited to the interiors of brachiopod shells (Fig. 9A, B). Two typical varieties of cements are present within unit F (Fig. 9). The first one comprises three generations, commonly occurring inside the shells (Fig. 9C–F). Firstly, red, fine-crystalline, fibrous dolomite (1) precipitated and rimmed the brown, laminated calcite related to the primary structure of bivalve shells. The next cement generation (2) corresponds to weakly luminescent anhydrite cement, rarely co-occurring with single, lenticular gypsum crystals exhibiting undulatory optical extinction (Fig. 9C). Anhydrite commonly occurs as veins, and its abundance increases towards the top of the section, where the transition from the Zechstein Limestone (Ca1) to the Lower Anhydrite (A1d) was documented (Fig. 1D). Finally, the youngest, zonal calcite cement developed (3; Fig. 9E, F). The zonal nature of calcite crystals is present in many variable arrangements. Locally, it is developed in a "flower-like" manner, while Figure 9F illustrates an example of a gastropod shell filled with purely zonal cements. The second variety of cement arrangement is related to brachiopod spines, whose internal structure was entirely replaced by two generations of cements (Fig. 9G, H). Yellow, sparry and isopachous calcite (I) rims an older generation of cement represented by fine crystalline dolosparite (II). These are postdated by the appearance of the youngest, sparry fluorite crystals located centrally in the interior of the bioclasts (Fig. 9H).

The intensity and frequency of the dissolution structures are unusual in comparison to the other units. Besides the dissolution voids observed under the polarizing microscope, also the macroscopic porosity and large caverns can be observed in the upper part of the unit (Fig. 4C). Mechanically compacted components occur again, here, in the form of deformed brachiopod spines, thus indicating the second stage of physical compaction. Since the horizontal stylolites are generally absent from the section of unit F, no significant evidence for chemical compaction is observed.

POROSITY

A combination of both fabric selective and not fabric selective porosities was encountered in the studied section. Poorly preserved, primary porosity is usually restricted to shelter voids (Fig. 10A, B). As long as intraparticle porosity is treated as primary porosity, it is an exception here, and occurs frequently
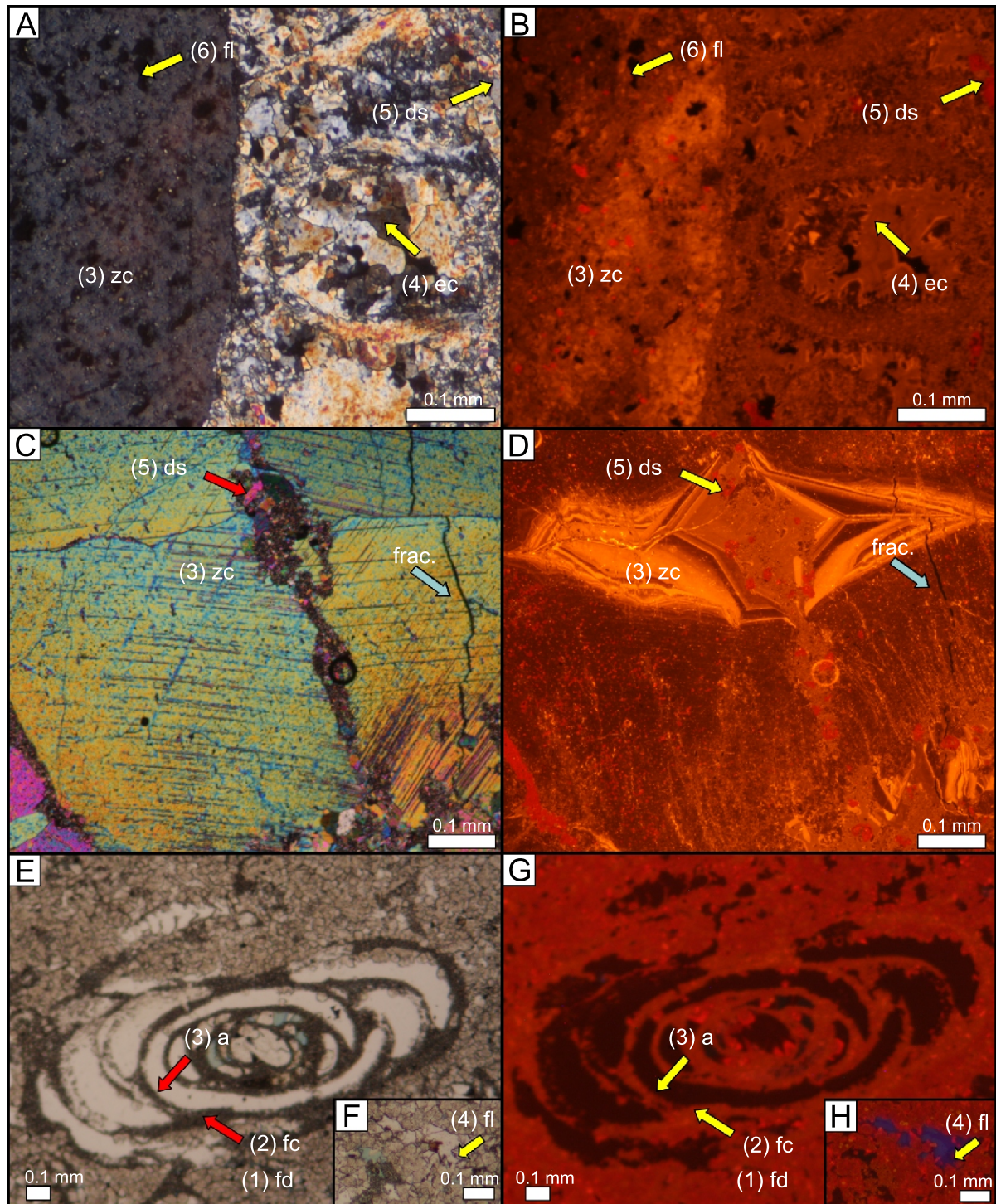
Fig. 7. Cementation and other diagenetic alterations in units C and D

A, B – cement generations of unit C (cf. Fig. 5E, F), note the appearance of equant calcite rimming a bioclast; **C, D** – the zonal calcite of unit C, intersected by finely-crystalline dolomite, note the presence of open fractures; **E–H** – unit D – wackestone with anhydrite and other cements filling the interior of foraminifers, note occasional occurrence of fluorite; A,C – cross-polarized light; E, F – plane-polarized light; B, D, G, H – cathodoluminescence; (1) corresponds to the oldest cement generation; fc – fibrous calcite; fd – fibrous dolomite; other explanations as in Figure 5
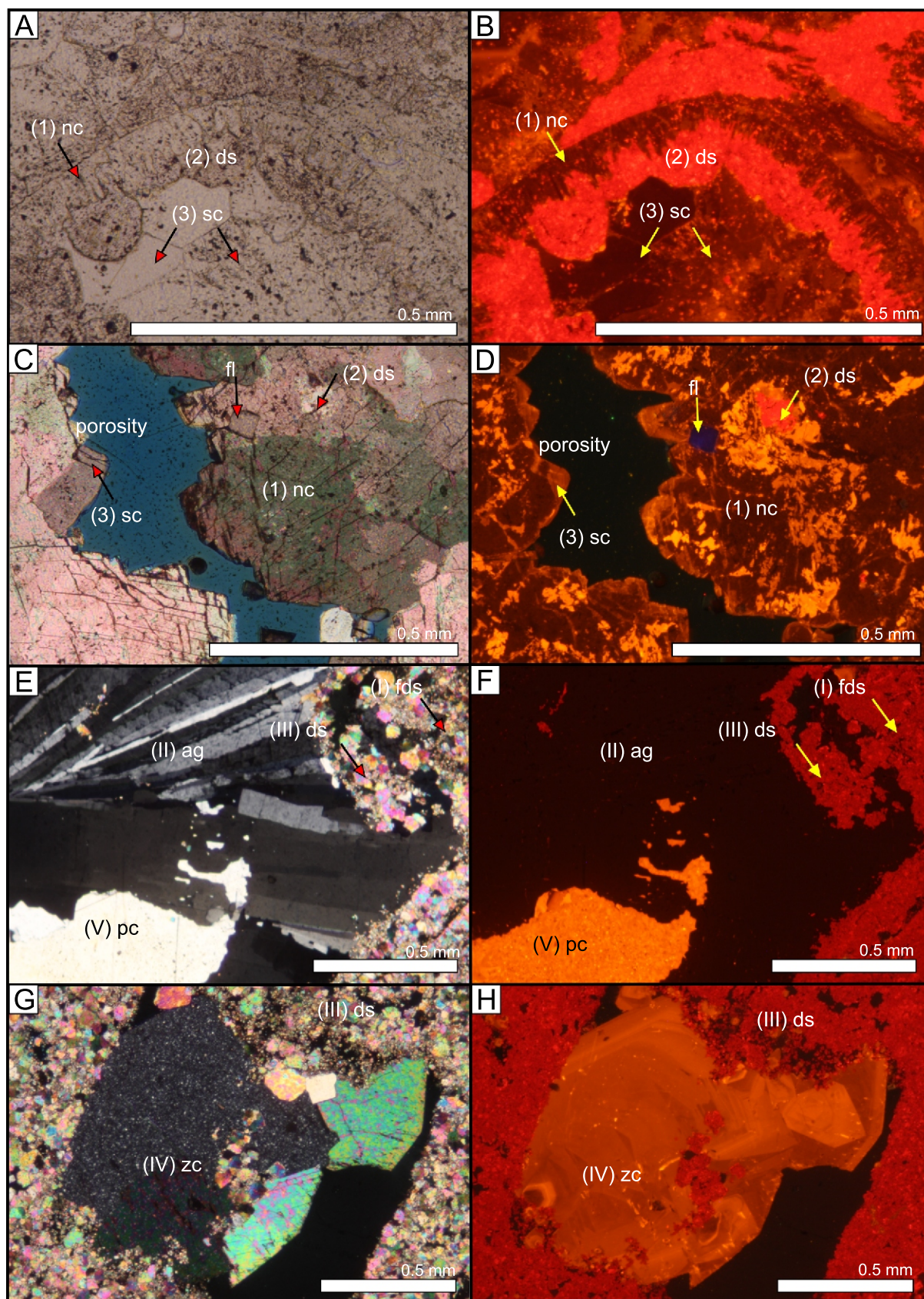
Fig. 8. Cementation and other diagenetic alterations in unit E

A, B – well-developed needle calcite accompanied by dolosparite and sparry calcite; C, D – cement sequence enriched by fluorite (cf. A, B); E, F – second set of cements – acicular gypsum replacing the interior of crinoids in a close neighborhood of poikilitic calcite and dolosparite; G, H – zonal calcite accompanied by vuggy and possible intercrystalline porosity and previously precipitated dolosparite; A, C – plane-polarized light; E, G: cross-polarized light; B, D, F, H – cathodoluminescence; (1) and (I) correspond to the oldest generation for a given set of cements, respectively; ag – acicular gypsum, pc – poikilitic calcite, sc – sparry calcite; other explanations as in Figure 5
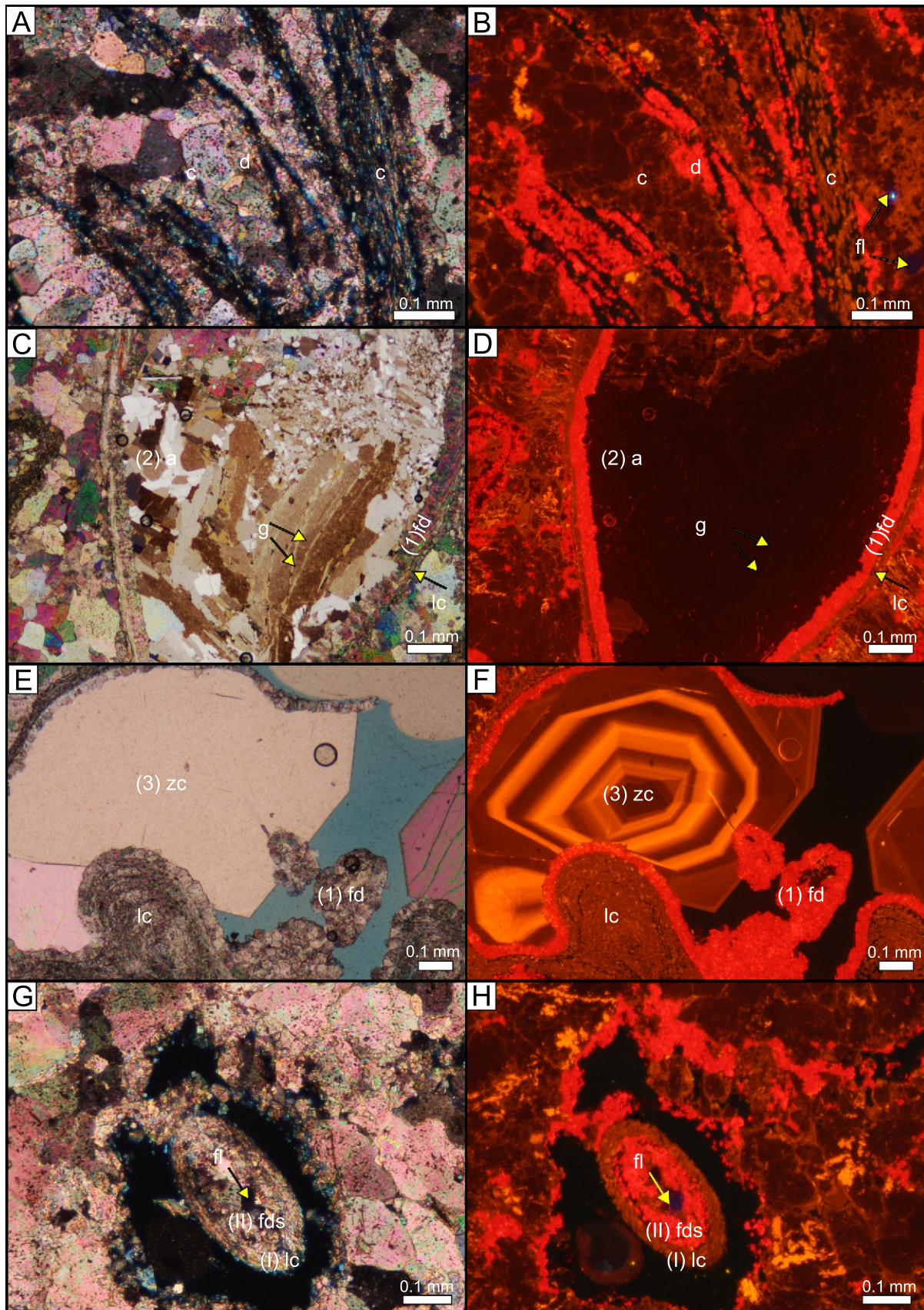
Fig. 9. Cementation and other diagenetic alterations in unit F

A, B – calcite and dolomite replacing a partially dissolved brachiopod shell (intraparticle porosity); **C, D** – three generations of cements in the interior of a bivalve, note the dominance of anhydrite, isopachous form of calcite cement and lenticular-like crystals of gypsum showing undulatory extinction; **E, F** – purely zonal interior of a gastropod shell (now represented by calcite), surrounded by partially dissolved (vug porosity) dolomite and laminated calcite; **G, H** – a set of cements developed within a brachiopod spine – black is vug porosity; A, C, E, G – cross-polarized light; B, D, F, H – cathodoluminescence; (1) and (I) correspond to the oldest generation of a given set of cements, respectively; c – calcite, lc – laminated (related to the primary structure of bivalve shell); other explanations as in Figure 5

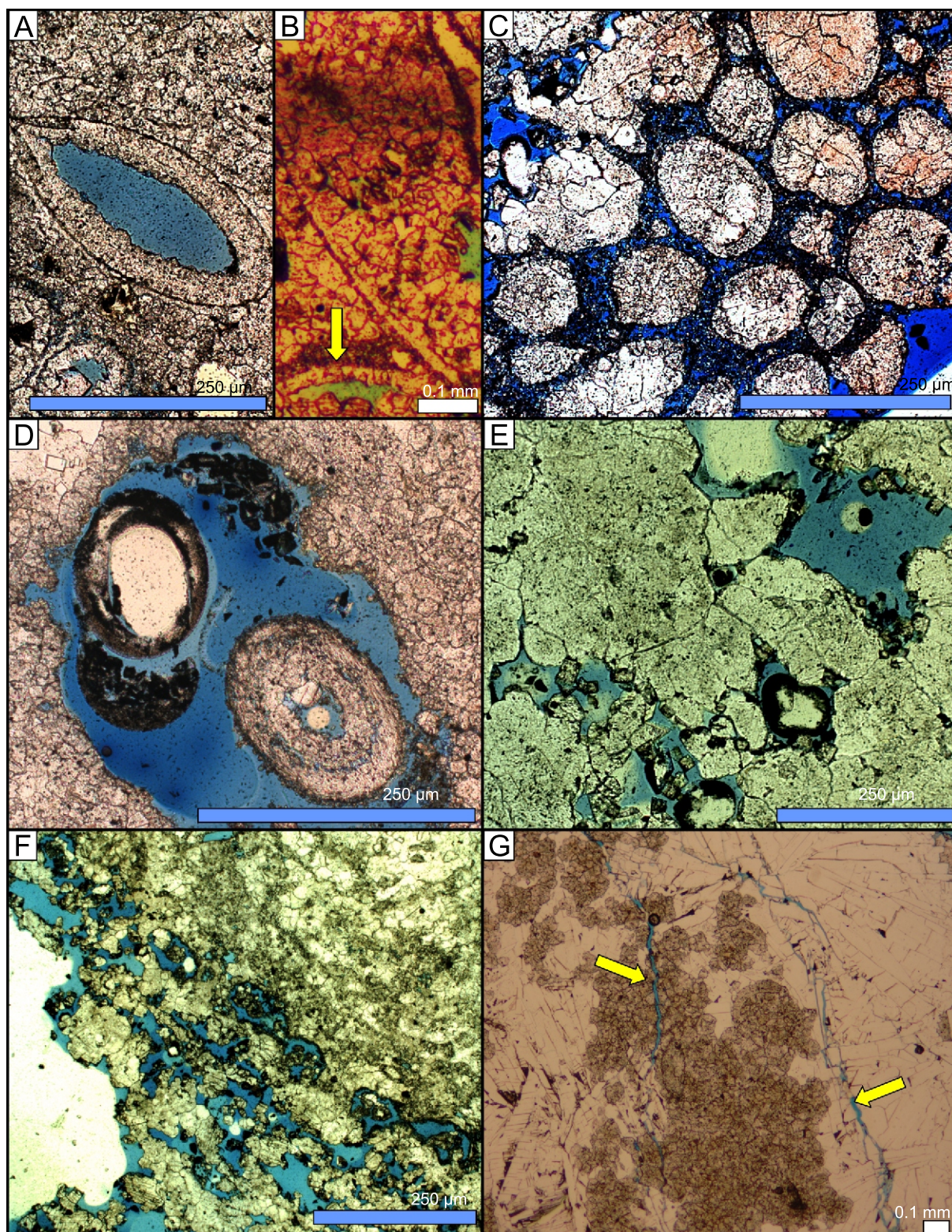**Fig. 10. Various porosity types encountered within the studied reef**

A – intraparticle/shelter inside an ostracod shell; **B** – shelter under a bivalve shell (arrowed); **C** – intraparticle within the bryozoan remnants; **D** – a dissolution vug; **E** – intercrystalline/vug; **F** – mouldic within the zoecial wall of a bryozoan; **G** – fracture (arrows); all photographs are taken in plane-polarized light

(Figs. 3F, H, 9A, B and 10C). Nevertheless, the dominance of secondary porosity is clearly visible.

Two main types of porosity are dominant in the Ca1 section. These are the vug (Figs. 9E, G and 10D) and intraparticle voids (Figs. 3F, H, 9A, B and 10C). Vugs are particularly well-developed in the upper part of the section. In few places, their size justifies distinguishing cavernous porosity (Fig. 4C). The role of the intercrystalline (Figs. 7E, G, 8G, H and 10E), interparticle, mouldic (Fig. 10F) and locally developed fracture porosity (Fig. 10G), however, also remains significant.

Unit B is represented by numerous pores of fracture origin. Another kind of porosity is represented by rarely distributed intercrystalline voids. The porosity is generally poorly developed within unit B, and this is due to a considerable influence of cementation. To obtain detailed porosity data for this unit, NMR studies were carried out. Owing to the NMR, the very low porosity of the unit was confirmed (Fig. 11A). This interval has the maximum effective porosity of just 2.8%, and its total porosity is only slightly higher (3%). The weakly developed pore system is related to larger voids showing longer T2 relaxation times. The capillary and clay-sized pores are negligible. The amplitude of the NMR signal shows many fluctuations that may result from diverse cementation.

The first type of porosity observed within unit C, is small dissolution vugs, occasionally reaching slightly greater sizes. Moreover, relatively low intercrystalline and interparticle porosity types developed in some places. Open fractures were also noted relatively frequently (Fig. 7C, D). Nevertheless, similarly as in case of unit B, this division does not exhibit higher porosity, either.

The pores of unit D are mostly of intercrystalline or interparticle nature (cf. Fig. 7E, F). The top of this unit shows hardly recognizable, lower porosity. It corresponds to a crystalline rock interval illustrated in Figure 3E.

Towards the top of the section, the porosity significantly increases. Unit E begins to show more and more abundant intraparticle porosity - developed in the interiors of the fauna (Fig. 3H). There also appear the first signs of the mouldic (cf. Fig. 10F), well-developed shelter (cf. Fig. 10A, B) and vuggy (cf. Fig. 10C) porosity. Additionally, intercrystalline porosity can also be observed in many places (Fig. 7G, H). The effective porosity investigated with the NMR equipment equals 12.8%, while the total porosity reaches 12.9% (Fig. 11B).

Finally, unit F was investigated in terms of porosity development. The wealth of its fossils, stays in accordance with the highly diverse porosity. As already mentioned, the dissolution vugs are most frequent in the upper part of the section (e.g., Fig. 9E). Within unit F, the intraparticle porosity is also extremely abundant (Fig. 10C). It is often due to bryozoan zoaria, whose interiors are partially dissolved. Moreover, signs of the mouldic porosity were encountered. This applies mostly to the shells of bivalves, fragments of zoecial walls of bryozoans and - in few places – to the shells of foraminifers, too.

The uppermost part of unit F, being represented by the transition from the Zechstein Limestone to the Lower Anhydrite (Fig. 1D), shows a negligible porosity. Except for this zone, the NMR effective porosity is quite high and reaches 8.1%. The total porosity was estimated to be the same as the effective one. It means that the capillary pore system does not exist in this case (Fig. 11C). It is probably absent from the whole reef, besides some minor exceptions observed within unit B (Fig. 11A).

DISCUSSION

Progressive subsidence (Kiersnowski et al., 2010) together with a consequently rising sea level (Strohmenger et al., 1996) created conditions favourable for the growth of the reef. The occurrence of three basic biofacies: the *Acanthocladia, Horridonia* and *Fenestella/Kingopora*, indicates that the reef has undergone quite a usual set of bathymetrical events. The initial transgression was rapid, and this is supported by the lacking carbonate breccia unit – proposed by Dyjaczynski et al. (2001) for reef rocks from the Kościan–Wielichowo region. Hence, the breccia might be eroded. Alternatively, the reef could not be close enough to the water surface at the beginning of the lowstand systems tract (LST), so that the subsequent transgression responsible for the formation of such breccias (D. Peryt et al., 2012), did not lead to its deposition. A relative sea level fall, in turn, occurred three times, ultimately leading to the meteoric exposure of the reef, significant karstification, and further sulphate platform development.

The reef was growing during deposition of the highstand systems tract (HST) (e.g., Wagner, 1988). Firstly, the *Acanthocladia* biofacies developed in a still relatively shallow, wave-affected environment. Abundant crinoids indicate that the water was of normal salinity (Peryt et al., 2012a; cf. Peryt and Peryt, 2012). The increased energy of water expressed by strongly fragmented bryozoan zoaria (cf. Scholle and Ulmer-Scholle, 2003) is slightly incoherent with Peryt's et al. (2012a) interpretation relating the *Acanthocladia* biofacies rather with moderate water energy. The highly energetic *Acanthocladia* is represented by filtering organisms that can tolerate a moderate rate of sediment supply, as well as a moderate amount of suspended matter present in water (Peryt et al., 2012a). Then, a subsequent sea level rise caused a change in the fauna, and allowed the appearance of *Horridonia*. The *Horridonia* biofacies is represented by sessile filtrators such as brachiopods and bryozoans (Peryt et al., 2012a). They might have inhabited the space below the storm wave base (e.g., Peryt et al., 2012a). These brachiopods preferred deeper and calmer waters than bryozoans of the *Acanthocladia* biofacies (e.g., Raczyński, 2000; Peryt et al., 2012a). Some of the brachiopod shells, however, are found in a position opposite to their growth. Such reworked shells seem to suggest a higher energy of water. The salinity was normal and the waters were of moderate depth.

When the sea level rose, a typical marine environment allowed the precipitation of aragonite, strengthening the structure of the reef. Aragonite, as a metastable phase (Sandberg, 1985), was replaced by calcite. The former presence of aragonite is expressed by the occurrence of needle-like calcite fringes preserved within the cements of unit B (e.g., Harris et al., 1985; Scholle and Ulmer-Scholle, 2003; D. Peryt et al., 2012; Peryt et al., 2012a). In the Wolsztyn Ridge region, like in the English and German parts of the Zechstein Basin (Paul, 1980; Tucker and Hollingworth, 1986), there are also botryoidal cements of primarily aragonitic origin (e.g., Peryt, 1984; Dyjaczynski et al., 2001; Weidlich, 2002; Peryt et al., 2012a; Jasionowski et al., 2014). Such structures are present within the previously described unit B. The marine character of currently calcitic cements can also be deduced on the basis of their frequently noted, isopachous character (e.g., Folk, 1965; Harris et al., 1985; Jasionowski et al., 2014). This type of cement was especially well-developed within unit F (see Fig. 9C, D, G, H).
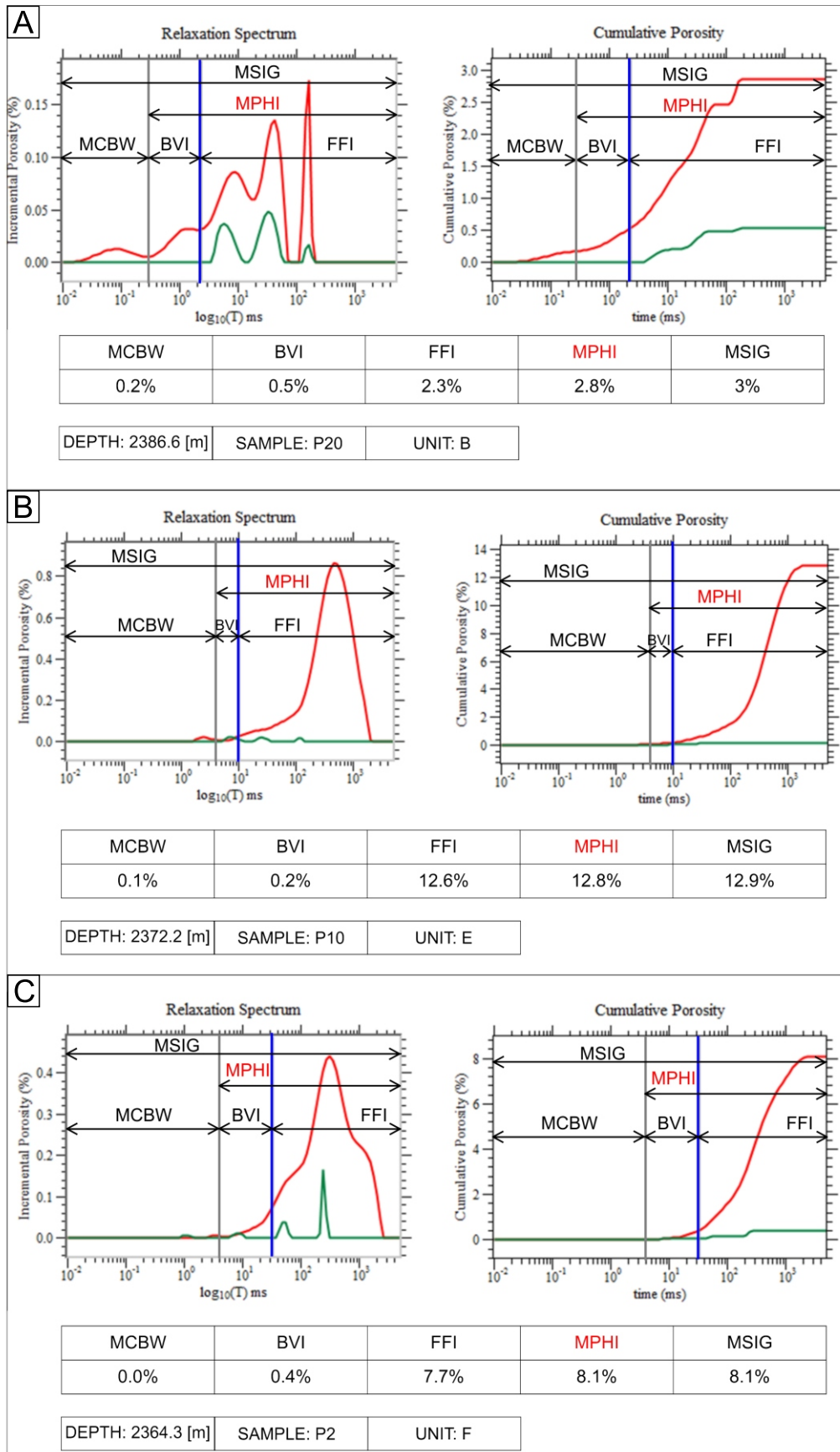
Fig. 11. The NMR porosity based on T2 relaxation time distribution

A – porosity of unit B; **B** – unit E; **C** – unit F; blue, vertical lines are the T2 cut-off values (separation of movable and irreducible fluids); grey, vertical lines are the cut-offs for Clay-Bound Water; red curves – saturated samples; green curves – dried samples; MCBW – Clay-Bound Water; BVI – Bulk Volume Irreducible (capillary water); FFI – Free Fluid Index; MPHI – NMR effective porosity; MSIG – NMR total porosity
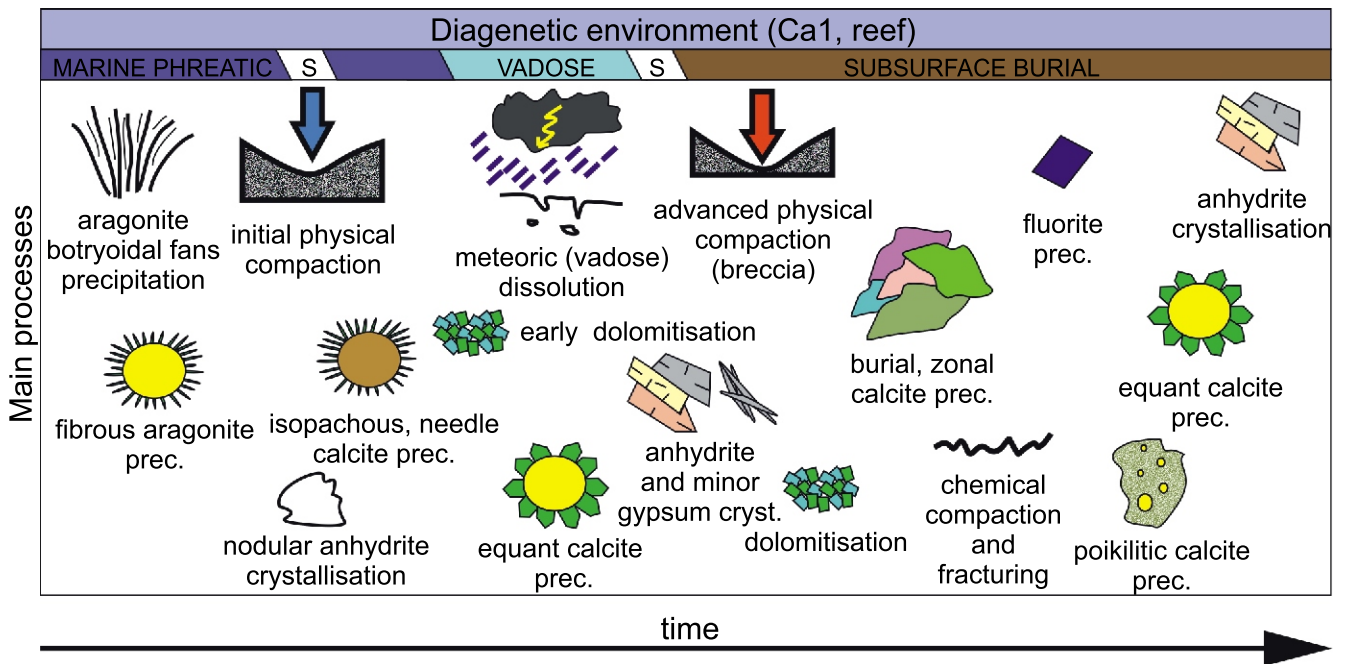
Fig. 12. Simplified diagenetic history of the Wielichowo isolated reef based on microscopic observations

S – sabkha environment

While the lower part of the reef was being affected by early diagenetic alteration, the living fauna occupying its top was represented by *Horridonia* biofacies. Then, the depth of the water decreased significantly, and consequently, the development of the renewed *Acanthocladia* biofacies started. In such conditions, brachiopods faced conditions unfavourable for their survival, so that their death was inevitable. Owing to this, bryozoans of the *Acanthocladia* biofacies could have easily attached themselves to an already preserved, partially lithified bottom, comprising formerly living brachiopods and other remnants of fossils (cf. Peryt et al., 2012a). Then, the already fallen sea level became even lower, thus allowing the appearance of the sabkha setting, expressed by anhydrite nodules, observed in the cores (Fig. 6A). The nodules significantly decreased the previously formed porosity. Among sulphates, anhydrite is most frequent, being most abundant in the upper part of unit D (Figs. 2 and 7E, G). Besides the sabkha setting, sulphates were probably deposited also in two different environments: (1) they precipitated after the dissolution of primary calcite/aragonite and secondary dolomite; and later (2) during further diagenetic stages, when the anhydrite crystallised in stylolites (cf. Fig. 6B). The sulphates co-occur with calcite and dolomite. The carbonates might have formed after exceptionally early sulphates, due to a short-lasting sea level rise, or later, during the burial of the strata.

The final facies transition from the *Acanthocladia* biofacies to the totally differently developed *Fenestella/Kingopora* biofacies indicates another relative sea level rise (cf. Peryt et al., 2012a). The *Fenestella/Kingopora* biofacies developed beneath the storm wave base. The waters were well oxidised and only slightly influenced by the presence of suspended organic matter. Deducing from the well-preserved and highly diverse fossils, the energy of water must have been relatively low. The organisms were living on a muddy bottom in a normal-salinity environment (Raczyński, 2000). In deep water conditions, isopachous calcite rims also precipitated, often surrounding the dolomitic cements. Such conditions were followed by a dramatic sea level fall, and hence the sabkha environment appeared again. As the result, the strata of the Werra Lower Anhydrite was deposited by the end of the lowstand systems tracts (LST) – see further discussion.

Another feature of the reef is the complexity of dolomitisation. It was multiphase and occurred in at least two different episodes (Figs. 5E, F and 12). The significant dolomitisation was preceded by early compaction, leading to deformation of the gentle, primarily calcitic or aragonitic brachiopod spines. Dolomite crystals usually form a stable and resistant framework, preventing the strata from compaction (Moore, 2001). Consequently, the presence of compacted grains suggests that they were deformed prior to the dolomitisation. Dolomitisation can occur in several different environmental conditions (Moore, 1989). Jasionowski et al. (2014) confirmed the complexity of multiphase dolomitisation in the Wolsztyn Ridge region. They interpreted the results of stable isotope geochemistry and related them to the particular episodes of the dolomitisation. Jasionowski et al. (2014) considered the sabkha environment to be responsible for allowing the precipitation of the majority of dolomite in this region. The dolomite could have originated owing to an increased reflux of fluids. Jasionowski et al. (2014) distinguished two basic types of dolomite: (a) dolomite replacing the previously precipitated calcite, and (b) dolomite having occurred in a form of cement. The isopachous geometry of some of the dolomitic cements might have originated in a marine (or vadose) setting and postdated calcite precipitation (Jasionowski et al., 2014). It should be added that both of dolomite types are present in the studied reef (for replacing dolomite see Figs. 3E and 5E, and for isopachous, fibrous dolomite see Figs. 8A, B and 9C–F). The earliest dolomitisation occurred within unit D, where it took place before the precipitation of fibrous calcite. In case of the remaining units, it postdated either the appearance of calcite (units: E, F) or sulphates (unit C). Such situation can be associated with a high content of both magnesium and calcium in sea water during the alteration of unit D. Moreover, the dolomite shows signs of dissolution.

Hence, it seems that its occurrence preceded the meteoric exposure.

As the reef became subaerially exposed, it has ultimately died. By the end of Zechstein Limestone deposition, a sea level fall took place once again, resulting in exposing the Ca1 strata. An abrupt transition from the Zechstein Limestone to the Lower Anhydrite is explained through a consequent sea level fall (Peryt, 1984; Wagner and Peryt, 1997; Mikołajewski et al., 2009; Kiersnowski et al., 2010). Since no stromatolitic unit (V) is present, this fall can be interpreted to have been rapid. Stromatolites are usually formed in a shallow, but still not subaerially exposed setting (Harris et al., 1985). However, they may have been eroded by wave activity. The sea level fall can be validated by the combination of growing proportion of anhydrite and the presence of ooids towards the top of the section (Fig. 2). Hence, it has been deduced that the diagenetic regime quickly changed from short-lasting shallow-marine to typical subaerial exposure.

Shortly after the activation of the first episode of dolomitisation, the reef was dynamically exposed to the influence of freshwater. Unit F seems to exhibit the strongest influence of the meteoric diagenesis among all of the distinguished textural divisions. It can be inferred based on numerous dissolution structures such as vugs, moulds and intraparticle pores, together with intercrystalline voids, often still remaining unfilled or only partially filled by the cements. Frequently occurring caverns, encountered in the upper part of this unit, can be treated as a proof of intense karstification, taking place in the vadose zone (e.g., Moore, 1989). The occurrence of vugs and moulds is due to activity of chemical dissolution during subaerial exposure, corresponding to the meteoric environment discussed above (e.g., Moore, 1989, 2001; Frykman et al., 1990; Scholle and Ulmer-Scholle, 2003; Ahr, 2008; Ali et al., 2010; Reijers, 2012). According to Dyjaczyński et al. (1997), the cavernous porosity occurs particularly within the Paproć and Kościan reefs. Comparing the obtained results with the Danish Zechstein carbonate reservoirs (Frykman et al., 1990), the occurrence of the dissolution vugs in both cases seems to be similar. However, in the investigated borehole, a much better developed association of intraparticle porosity was encountered. Frykman et al. (1990) reported that the intercrystalline porosity rather occurred in their study area, and tied it with the primary porosity. The intraparticle porosity is considered as primary (e.g. Moore, 2001; Mazzullo, 2004), but it is also believed to express the activity of dissolution processes (e.g., Frykman et al., 1990; Flügel, 2010). The fracture porosity is relatively well-developed and surely accounts for the permeability and porosity of the reef.

Equant calcite appeared simultaneously with the meteoric dissolution, often surrounding the stems of crinoids. It is supposed to indicate the influence of the vadose zone on the cementation development (e.g., Ahr, 2008). Such situation takes place mainly within unit B.

Subsequently, the reef strata were being successfully buried and overlain by evaporites of the Lower Anhydrite (A1d) regarded to be a lowstand systems tract (LST) sediment (e.g., Peryt and Wagner, 1998; Peryt, 2010). By the end of the LST, the sea level started to rise (cf. Catuneanu, 2006). This initiated a quick sulphate platform development. The sulphate platform might have been developed on the previously, subaerially exposed reef buildup. Then, continuous flooding and a possible seepage (Kendall, 2010), allowed thick assemblages of halite (Na1; e.g., Peryt, 2010) to fill the depressions located near the uplifted tectonic blocks. A diversified relief and accommodation space available for halite deposition might have also been inherited after locally activated tectonics (Kiersnowski et al., 2010).

When the reef strata became buried, physical compaction was intensified significantly as can be explained on the example of the intraclastic breccia of unit E. It is claimed that such structures were formed due to a dramatically rapid and huge sediment load (cf. Scholle and Ulmer-Scholle, 2003). The intraclastic breccia of unit E, is bounded from the top by the cement composed of dolomite rhombohedra that have not prevented the breccia from compaction. It can only be explained based on a theory that the dolomitisation occurred after its deposition in this case. It might have been induced by the seepage of marine water, as illustrated by Moore (1989).

Burial cementation was activated simultaneously with physical compaction. This is expressed by the occurrence of well-developed, sparry and zonal calcite cements, particularly well-visible within unit F. Scholle and Ulmer-Scholle (2003) related such cements with the burial conditions. As the subsurface burial continued, the chemical compaction became active, too. As a result of this process, numerous horizontal stylolites were formed. The rocks of unit B are the best example of the occurrence of the chemical compaction. This phenomenon was also observed in the shallower parts of the section, but its intensity was incomparably weaker.

The fractures cutting the earlier cements were created due to increased stress conditions (cf. Ahr, 2008; Fossen, 2010). Because some of them remained unfilled, they might have significantly enhanced the porosity and permeability of the potential reservoir. The occurrence of the fractures partially filled by anhydrite within units E and F is compatible with their characterisation provided by Peryt et al. (2012a). Raczyński (2000) noticed that the porosity reduction caused by the precipitation of sulphates is diversified and exhibits a variable intensity. Within units E and F, however, fractures are of negligible significance, as they are either poorly developed or monotonously filled with anhydrite. The chemical compaction and fracturing were postdated by the fluorite occurrence (e.g., Fig. 8D). Ahr (2008) associated the presence of such "exotic" minerals with burial conditions. The position of the fluorite crystals, which are always located inside other cements or grains, verifies its youngest age. It is worth adding, that in many cases, fluorite has significantly decreased the intercrystalline, depositional porosity.

Subsequently, poikilitic calcite formed (Fig. 8E, F) possibly due to a contact with the hyposaline waters (of decreased salinity; Folk and Siedlecka, 1974). Alternatively, elevated temperatures and pressure dissolution might have been responsible for its precipitation (cf. Heydari and Moore, 2006).

Last but not least, equant, sparry calcite cement was developed (see Fig. 8A, B). It must have been formed during the burial of the strata (cf. Melim et al., 2002), because this type of calcite was found in the deepest parts of the reef, not showing any evident signs of subaerial exposure.

CONCLUSIONS

1. The 26-m-thick reef carbonates of the Zechstein Limestone in the Wielichowo-8 borehole are lacking two units proposed earlier for reefs of the Kościan–Wielichowo region (Dyjaczynski et al., 2001); these are the bottommost carbonate breccia unit (I), whose absence is interpreted to be due to either relatively elevated water table during the initial transgression from the Barents Sea, or wave erosion; and the topmost stromatolitic-pisolitic unit (V), probably absent because of the rapid sea level fall.

2. There were three major sea level falls – the first one during the transition from the relatively deep *Horridonia* biofacies to the shallow-water *Acanthocladia* biofacies, the second one during the first episode of sabkha sedimentation, marked by the nodular anhydrite crystallisation, and finally, when a dynamic sea level fall occurred after the sedimentation of the deep-water *Fenestella/Kingopora* biofacies, thus leading to the second sabkha episode. The last-mentioned, dramatic sea level fall, had enabled the aggressive, CO_2 rich fluids to dissolve the previously formed cements and fossils, before the sulphate platform was developed.

3. Aragonite precipitation, marked by the occurrence of the botryoidal fans and needle calcite fringes, has strengthened the framework of the reef and allowed its growth. The diagenesis, though dominated by its early stages, was relatively complex and the processes such as dissolution, replacement, recrystallisation, cementation, dolomitisation, fracturing and both chemical and physical compaction had a significant influence on final porosity character. The primary porosity was significantly reduced by physical and chemical compaction. The dolomitisation expected to form a stable framework preventing the strata from compaction, occurred too late to act this way. Additionally, the sulphate cementation has also accounted for porosity reduction. Consequently, the porosity is predominantly developed as big dissolution caverns, observed within with the E and F units, ensuring an elevated effective NMR porosity reaching 12.8%. Among the porosity types, the meteoric vugs created during the last sea level fall dominate.

REFERENCES

Ahr, W.M., 2008. Geology of Carbonate Reservoirs. The Identification, Description and Characterization of Hydrocarbon Reservoirs in Carbonate Rocks. John Wiley & Sons, Inc. Publication, Hoboken.

Akkurt, R., Bachman, H.N., Minh, C.C., Flaum, C., LaVigne, J., Leveridge, R., Carmona, R., Crary, S., Decoster, E., Heaton, N., Hürlimann, M.D., Looyestijn, W.J., Mardon, D., White, J., 2009. Nuclear magnetic resonance comes out of its shell. Oilfield Review, Schlumberger, **20**.

Ali, A.S., Clark, W.J., Dribus, J.R., 2010. Diagenesis and reservoir quality. Oilfield Review, Schlumberger, **22**: 14–27.

Biernacka, J., Borysiuk, K., Raczyński, P., 2005. Zechstein (Ca1) limestone-marl alternations from the North-Sudetic Basin, Poland: depositional or diagenetic rhythms? Geological Quarterly, **49** (1): 1–14.

Catuneanu, O., 2006. Principles of Sequence Stratigraphy. Elsevier Science.

Choquette, P.W., Pray, L.C., 1970. Geological nomenclature and classification of porosity in sedimentary carbonates. AAPG Bulletin, **54**: 207–250.

Coates, G.R., Lizhi, X., Manfred, G.P., 1999. NMR Logging Principles and Applications. Halliburton Energy Services, USA.

Dunham, R.J., 1962. Classification of carbonate rocks according to depositional texture. AAPG Memoir, **1**: 108–121.

Dyjaczyński, K., Peryt, T.M., 2014. Controls on basal Zechstein (Wuchiapingian) evaporite deposition in SW Poland. Geological Quarterly, **58** (3): 485–502.

Dyjaczyński, K., Mamczur, S., Radecki, S., 1997. New perspectives for gas deposits' prospection within the Zechstein Limestone strata, Foresudetic Monocline (in Polish with English summary). Przegląd Geologiczny, **45**: 1248–1256.

Dyjaczynski, K., Górski, M., Mamczur, S., Peryt, T.M., 2001. Reefs in the basinal facies of the Zechstein Limestone (upper Permian) of western Poland: a new gas play. Journal of Petroleum Geology, **24**: 265z–285.

Evamy, B.D., 1963. The application of a chemical staining technique to a study of dedolomitisation. Sedimentology, **2**: 164–170.

Flügel, E., 2010. Microfacies of Carbonate Rocks. Analysis, Interpretation and Application: 267–338. Springer, Berlin.

Folk, R.L., 1965. Some aspects of recrystallization in ancient limestones. SEPM Special Publication, **13**: 14–48.

Folk, R.L., Siedlecka, A., 1974. The "schizohaline" environment: its sedimentary and diagenetic fabrics as exemplified by Late Paleozoic rocks of Bear Island. Svalbad. Sedimentary Geology, **11**: 1–15.

Fossen, H., 2010. Structural Geology. Cambridge University Press, Cambridge.

Frykman, P., Stentoft, N., Rasmussen, K.L., Christensen, O.W., Andersen, P.V., Jacobsen, F.L., 1990. Diagenesis and porous system in Danish Zechstein carbonate reservoirs. Geological Survey of Denmark Thoravej, **31**: 1–107.

Gast, R.E., 1988. Rifting im Rotliegenden Niedersachsens. Geowissenschaften, **4**: 115–122.

Hara, U., Słowakiewicz, M., Raczyński, P., 2013. Bryozoans (trepostomes and fenestellids) in the Zechstein Limestone (Wuchiapingian) of the North Sudetic Basin (SW Poland): palaeoecological implications. Geological Quarterly, **57** (3): 417–432.

Harris, P.M., Kendall, C.G.St.C., Lerche, I., 1985. Carbonate cementation – a brief review. SEPM Special Publication, **36**: 79–95.

Heydari, E., Moore, C.H., 2006. Zonation and geochemical patterns of burial calcite cements; upper Smackover Formation, Clarke County, Mississippi. Journal of Sedimentary Research, **63**: 44–60.

Jasionowski, M., Peryt, T.M., Durakiewicz, T., 2014. Polyphase dolomitisation of the Wuchiapingian Zechstein Limestone (Ca1) isolated reefs (Wolsztyn Palaeo-Ridge, Fore-Sudetic Monocline, SW Poland). Geological Quarterly, **58** (3): 503–520.

Karnkowski, P.H., 1999. Origin and evolution of the Polish Rotliegend Basin. Polish Geological Institute Special Papers, **3**.

Kendall, A.C., 2010. Marine evaporites. Geol. Assoc., GeoText, **6**: 503–537. Canada.

Kiersnowski, H., Paul, J., Peryt, T.M., Smith, D.B., 1995. Facies, paleogeography, and sedimentary history of the Southern Permian Basin in Europe. The Permian of Northern Pangea, **2**: 119–136. Springer, Berlin.

Kiersnowski, H., Peryt, T.M., Buniak, A., Mikołajewski, Z., 2010. From the intra-desert ridges to the marine carbonate island chain: middle to late Permian (Upper Rotliegend–Lower Zechstein) of the Wolsztyn-Pogorzela high, west Poland. Geological Journal, **44**: 319–335.

Kotarba, M.J., Peryt, T.M., Kosakowski, P., Więcław, D., 2006. Organic geochemistry, depositional history and hydrocarbon generation modelling of the Upper Permian Kupferschiefer and Zechstein Limestone strata in south-west Poland. Marine and Petroleum Geology, **23**: 371–386.

Mazzullo, S.J., 2004. Overview of porosity evolution in carbonate reservoirs. Kansas Geological Society Bulletin, **79**: 22–27.

Melim, L.A., Westphal, H., Swart, P.K., Eberli, G.P., Munnecke, A., 2002. Questioning carbonate diagenetic paradigms: evidence from the Neogene of the Bahamas. Marine Geology, **185**: 27–53.

Mikołajewski, Z., Buniak, A., Chmielowiec-Stawska, A., 2009. Reservoir properties of reef sediments of the Zechstein Limestone (Ca1) at the example of the Brońsko gas field (in Polish). Przegląd Geologiczny, **57**: 309–310.

Moore, C.H., 1989. Carbonate Diagenesis and Porosity. Developments in Sedimentology, **46**. Elsevier Science, Amsterdam.

Moore, C.H., 2001. Carbonate Reservoirs. Porosity Evolution and Diagenesis in a Sequence Stratigraphic Framework. Developments in Sedimentology, **55**. Elsevier Science, Amsterdam.

Paul, J., 1980. Upper Permian algal stromatolite reefs, Harz Mountains (F.R. Germany). Contributions to Sedimentology, **9**: 253–268.

Peryt, D., Peryt, T.M., Raczyński, P., Chłódek, K., 2012. Foraminiferal colonization related to the Zechstein (Lopingian) transgression in the western part of the Wolsztyn Palaeo-Ridge area, Western Poland. Geological Quarterly, **56** (3): 529–546.

Peryt, T.M., 1981. Former aragonitic submarine hemispheroids associated with vadose deposits, Zechstein Limestone (Upper Permian), Fore-Sudetic area, western Poland. Neues Jahrbuch für Geologie und Paläontologie Monatshefte, **9**: 559–570.

Peryt, T.M., 1984. Sedimentation and early diagenesis of the Zechstein Limestone in Western Poland (in Polish with English summary). Prace Instytutu Geologicznego, **109**: 1–80.

Peryt, T.M., 2010. Zechstein 1-3 evaporites of the Gorzów Block (NW Poland) (in Polish with English summary). Przegląd Geologiczny, **58**: 689–694.

Peryt, T.M., Peryt, D., 2012. Geochemical and foraminiferal records of environmental changes during Zechstein Limestone (Lopingian) deposition in Northern Poland, Geological Quarterly, **56** (1): 187–198.

Peryt, T.M., Wagner, R., 1998. Zechstein evaporite deposition in the Central European Basin: cycles and stratigraphic sequences. Journal of Seismic Exploration, **7**: 201–218.

Peryt, T.M., Ważny, H., 1980. Microfacies and geochemical development of the basin facies of the Zechstein Limestone (Ca1) in western Poland. Contributions to Sedimentology, **9**: 279–306.

Peryt, T.M., Raczyński, P., Peryt, D., Chłódek, K., 2012a. Upper Permian reef complex in the basinal facies of the Zechstein Limestone (Ca1), western Poland. Geological Journal, **47**: 5375–52.

Peryt, T.M., Durakiewicz, T., Kotarba, M.J., Oszczepalski, S., Peryt, D., 2012b. Carbon isotope stratigraphy of the basal Zechstein (Lopingian) strata in Northern Poland. Geological Quarterly, **56** (2): 285–298.

Peryt, T.M., Hałas, S., Peryt, D., 2015. Carbon and oxygen isotopic composition and foraminifers of condensed basal Zechstein (Upper Permian) strata in western Poland: environmental and stratigraphic implications. Geological Journal, **50**: 446–464.

Pharaoh, T.C., Dusar, M., Geluk, M., Kockel, F., Krawczyk, C., Krzywiec, P., Scheck -Wenderoth, M., Thybo, H., Vejbaek, O., Wees, J.-D., van, 2010. Tectonic evolution. In: Petroleum Geological Atlas of the Southern Permian Basin Area (eds. J.C. Doornenbal and A.G. Stevenson): 25–58. EAGE Publications b.v., Houten.

Pikulski, L., Wolnowski, T., 2005. Geological analysis of the Zechstein Limestone formations (Ca1) in Western Poland. AAPG Search and Discovery. AAPG/EAGE International Research Conference, El Paso, Texas, October 1–5.

Raczyński, P., 2000. Associations of organisms in the Zechstein Limestone (Ca1) reef complex on the Wolsztyn Ridge (in Polish). Przegląd Geologiczny, **48**: 469–470.

Reijers, T.J.A., 2012. Sedimentology and diagenesis as 'hydrocarbon exploration tools' in the Late Permian Zechstein-2 Carbonate Member (NE Netherlands). Geologos, **18**: 163–195.

Sandberg, P., 1985. Aragonite cements and their occurrence in ancient limestones. SEPM Special Publication, **36**: 33–57.

Scholle, P.A., Ulmer-Scholle, D.S., 2003. A color guide to the petrography of carbonate rocks: grains, textures, porosity, diagenesis. AAPG Memoir, **77**.

Smith, D.B., 1980. The evolution of the English Zechstein basin. Contributions to Sedimentology, **9**: 7–34.

Strohmenger, C., Antonnini, M., Jäger, G., Rockenbauch, K., Strauss, C., 1996. Zechstein 2 Carbonate reservoir facies distribution in relation to Zechstein sequence stratigraphy (Upper Permian, Northeast Germany): an integrated approach. Bulletin des Centres de Recherches Exploration – Production Elf-Aquitaine, **20**: 1–35.

Tucker, M.E., Hollingworth, N.T.J., 1986. The Upper Permian Reef Complex (EZI) of North East England: Diagenesis in a marine to evaporitic setting. In: Reef Diagenesis (eds. J.H. Schroeder and B.H. Purser): 270–290. Springer, Berlin.

Wagner, R., 1988. The evolution of the Zechstein Basin in Poland (in Polish with English summary). Kwartalnik Geologiczny, **32** (1): 33–52.

Wagner, R., Peryt, T.M., 1997. Possibility of sequence stratigraphic subdivision of the Zechstein in the Polish Basin. Geological Quarterly, **41** (4): 457–474.

Weidlich, O., 2002. Middle and Late Permian reefs – distributional patterns and reservoir potential. SEPM Special Publication, **72**: 339–390.

Ziegler, P.A., 1990. Geological Atlas of Western and Central Europe, 2nd edition. Shell Internationale Petroleum Maatschappij B.V, Hague.